Centralized Control for Parallel Operation of Distributed Generation Inverters in Microgrids

K. T. Tan, *Student Member, IEEE*, X. Y. Peng, *Student Member, IEEE*, P. L. So, *Senior Member, IEEE*, Y. C. Chu, *Senior Member, IEEE*, and M. Z. Q. Chen, *Member, IEEE*

***Abstract*—This paper presents a centralized control system that coordinates parallel operations of different distributed generation (DG) inverters within a microgrid. The control design for the DG inverters employs a new Model Predictive Control algorithm that allows faster computational time for large power systems by optimizing the steady-state and the transient control problems separately. An overall energy management system is also implemented for the microgrid to coordinate load sharing among different DG units during both grid-connected and islanded operations. The design concept of the proposed control system is evaluated through simulation studies under different test scenarios. The impact of the increased penetration of DG units on the distribution grid is also investigated using the proposed microgrid. The simulation results show that the operations of the DG units within the microgrid can be coordinated effectively under the proposed control system to ensure stable operation of the overall microgrid.**

***Index Terms*—Centralized control, distributed generation, energy management, microgrids, parallel inverter operation.**

I. Introduction

THE liberalization of the electricity market and the integration of advanced communication and information technologies into the power industry have attracted widespread adoption on the microgrid concept. The microgrid concept offers customers increased reliability and quality in the service provided by utility companies. The reduction in global emissions and energy losses also make the microgrid a promising alternative to traditional power distribution systems [1]–[3]. However, the design of a microgrid architecture that provides an efficient operation poses a challenging problem.

This paper aims to develop an efficient control and energy management system (EMS) for a microgrid consisting of different distributed generation (DG) units operating in parallel to ensure smooth operation of the microgrid during both grid-connected and islanded operations. The controller must allow parallel operation of several inverters using voltage and frequency droop control to ensure proper load sharing during islanded operation [4]–[8]. With the proliferation of power electronics equipment being connected to the microgrid, the load current is usually distorted due to the presence of harmonic components. The DG units are also designed to improve the power quality of the distribution network by compensating for harmonic currents. The integration of DG units in the distribution grid will lead to a more complex flow of real and reactive power, which can change the voltage profile at the load side during normal operations, and a more complex flow of fault currents for any fault occurring in the microgrid [9]. Hence, the impact of the increased penetration of DG units on the existing distribution grid needs to be studied.

The model of the DG interfacing inverters and an overall EMS based on a centralized control strategy for the microgrid are developed to coordinate the parallel operations of the different DG units. The EMS controls and monitors different aspects of power management such as load forecasting, unit commitment, economic dispatch and optimal power flow through a centralized server. Important information such as field measurements from smart meters, transformer tap positions and circuit breaker (CB) status are all sent to the centralized server for processing through Ethernet.

Many research works on designing the controllers for parallel operation of DG inverters in a microgrid during grid-connected and islanded operations have been conducted [7], [8], [10]. A commonly adopted control scheme which is detailed in [7], [8] contains an inner voltage and current loop and an external power loop to regulate the output voltage and the power flow of the inverters. In [10], a control scheme which uses separate controllers for the inverters during grid-connected and islanded operations is proposed. The scopes of these research works are focused primarily for linear loads. To increase the robustness of the controller with respect to load disturbances and parameter variations, this paper proposes a model-based controller using a newly developed Model Predictive Control (MPC) algorithm for the DG inverters.

The MPC algorithm tracks periodic reference signals for fast sampling linear time-invariant (LTI) systems that are subject to input constraints. This control methodology decomposes the control problem into steady-state and transient subproblems that are optimized separately. Apart from the conventional formulation based on the control inputs as variables, a parameterization using a dynamic policy on the inputs is also introduced. In this way, the computational time is greatly reduced.

Investigations will be conducted using the proposed microgrid and its control system on the following technical issues:

1) power quality improvement in the distribution grid;
2) real and reactive power management during grid-connected and islanded operations;
3) network voltage changes; and
4) increased fault levels.

Manuscript received December 19, 2011; revised March 22, 2012, May 19, 2012; accepted June 15, 2012. Date of publication August 14, 2012; date of current version December 28, 2012. This work was supported by the School of Electrical and Electronic Engineering, Nanyang Technological University, Singapore, and also by A*STAR under the Smart Grid Project (SERC Grant No. 112 120 2022). The work of M. Z. Q. Chen and Y. C. Chu was supported by HKU CRCG Fund 201111159110. The work of M. Z. Q. Chen was also supported by NNSFC 61004093. Paper no. TSG-00690-2011.

The authors are with Nanyang Technological University, Singapore 639798, and also with the University of Hong Kong, Hong Kong, China (e-mail: eplso@e.ntu.edu.sg).

Digital Object Identifier 10.1109/TSG.2012.2205952

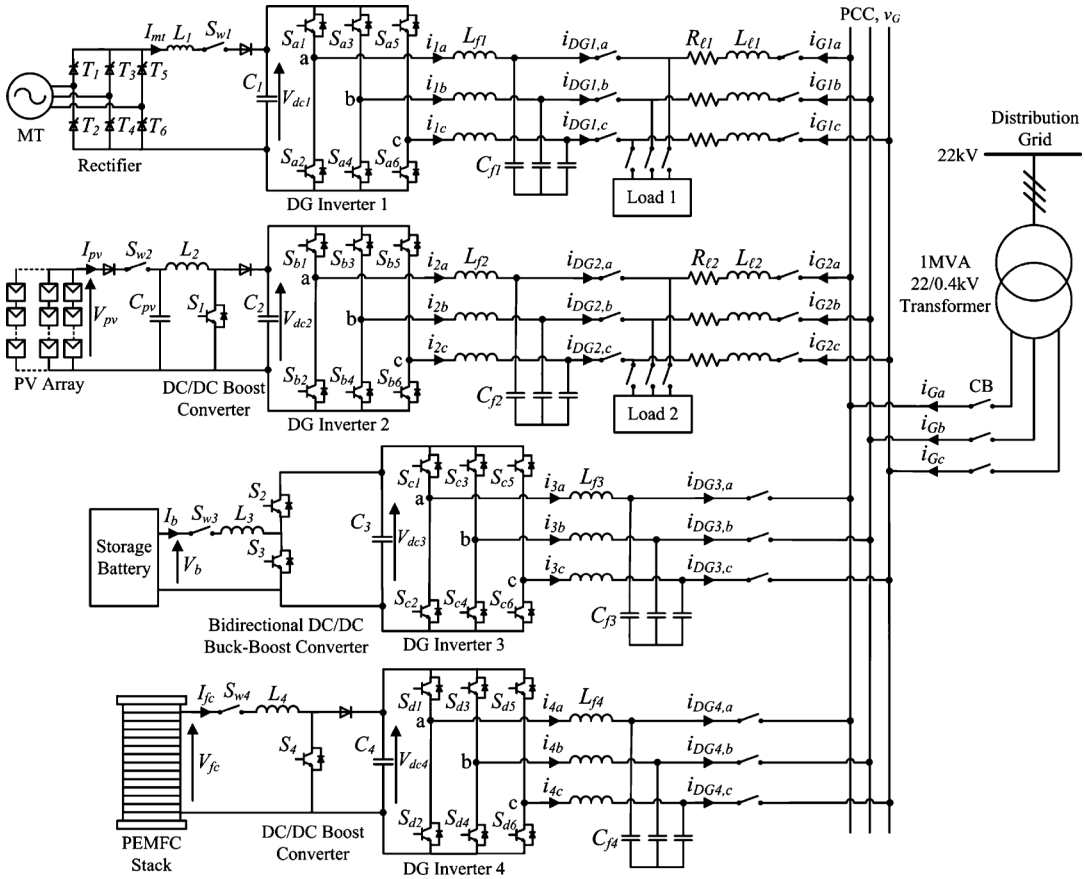

Fig. 1. Overall configuration of the proposed microgrid architecture.

II. System Description and Modeling

A. System Description

Fig. 1 shows the configuration of the proposed microgrid designed to operate either in the grid-connected or islanded mode. The proposed microgrid consists of a 15 kVA microturbine (MT), a 5 kWp (kilowatt-peak) photovoltaic (PV) array, a 20 Ah lithium-ion storage battery (SB), and a 5 kW proton exchange membrane fuel cell (PEMFC) stack. The MT and the PV array function as the main DG units of the microgrid. The SB and the PEMFC stack are incorporated as back-up DG units for the PV array and will supply power for any shortage in the generated power to ensure stable operation of the overall microgrid. During off-peak periods, the cost of generation from the distribution grid is lower; hence, the SB is charged up by the distribution grid. Conversely, the SB can deliver power into the microgrid at times of high generation cost to achieve peak shaving.

During grid-connected operation, the microgrid is connected to the distribution grid at the point of common coupling (PCC) through a CB. The main DG units provide local power and voltage support for the loads and hence reduce the burden of generation and delivery of power directly from the distribution grid. With the proliferation of power electronics equipment being connected to the microgrid, the load currents could be distorted due to the presence of harmonic components. The DG units also compensate for any harmonics in the currents drawn by nonlinear loads in the microgrid to prevent the harmonics from propagating to other electrical networks that are connected to the PCC.

When a fault occurs on the upstream network of the distribution grid, the CB disconnects the microgrid from the distribution grid. The DG units are now the sole power sources left to supply the loads. When the generation capacity of the main DG units is unable to meet the total load demand, the SB and the PEMFC stack can provide for the shortage in real and reactive power to maintain the power balance and voltage stability of the microgrid.

B. Grid Operation

The dc-link voltages of the DG inverters are regulated by their respective rectifier, dc/dc boost converter, and bidirectional dc/dc buck-boost converter at a desired voltage as seen in Fig. 1 and the respective DG unit will deliver the necessary power to maintain the power balance in the dc-link.

During grid-connected operation, the power balance of the overall distribution system is achieved through the distribution grid. However, when the microgrid transits to operate islanded from the distribution grid, the SB and the PEMFC stack can maintain the power balance in the distribution system according to the following power balance equation:

$$P_{\rm mt} + P_{\rm pv} + P_b + P_{\rm fc} = P_L \tag{1}$$

where $P_{\rm mt}$ and $P_{\rm pv}$ are the powers delivered by the MT and the PV array, respectively, P_b is the SB power subjected to the charging and discharging constraints given by

$$P_b \le P_{b,\max}. \tag{2}$$

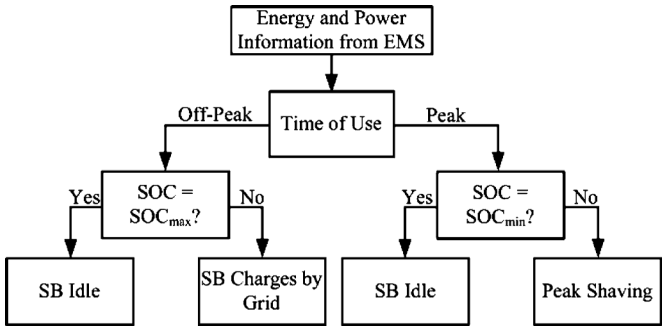

Fig. 2. Operation of the SB during grid-connected operation.

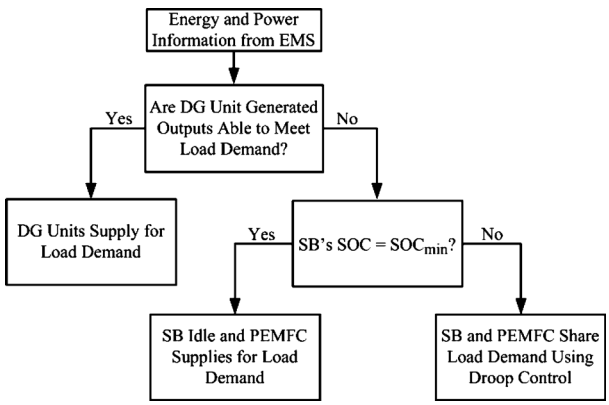

Fig. 3. Operation of the SB and PEMFC stack during islanded operation.

$P_{\rm fc}$ is the power delivered by the PEMFC stack and P_L is the real power delivered to the loads. The energy constraints of the SB are determined based on the state-of-charge (SOC) limits given by

$$\mathrm{SOC}_{\min} < \mathrm{SOC} \leq \mathrm{SOC}_{\max}. \tag{3}$$

Although the SOC of the SB cannot be measured directly, it can be determined through several estimation methods [11]–[13]. In grid-connected operation, if the SOC of the SB is below the limit $\mathrm{SOC}_{\max}$, the SB can be charged by the distribution grid during off-peak periods. When the microgrid operates islanded from the distribution grid, the SB can operate in the charging, discharging or idle mode depending on its SOC. The load demand will be shared appropriately using a droop control method, which will be elaborated further in Section II-D. The flowcharts in Figs. 2 and 3 summarize the operations of the SB and the PEMFC stack based on the output information provided by an EMS during grid-connected and islanded operations, respectively.

C. DG Inverter Modeling

Fig. 4 shows the equivalent single-phase representation of the DG inverter of the MT or PV array during grid-connected operation, whereas Fig. 5 shows the DG inverters of the SB and PEMFC stack during islanded operation [6], [10], [14]. The switched voltage across the output of the DG inverter is represented by $u_j V_{dcj}$, where u_j is the control input and $j = 1, 2, 3, 4$. In Fig. 4, the output of the DG inverter is interfaced with an LC filter represented by L_{fj} and C_{fj}, to eliminate the high switching frequency harmonics generated by the DG inverter. The resistance R_{fj} models as the loss of the DG inverter.

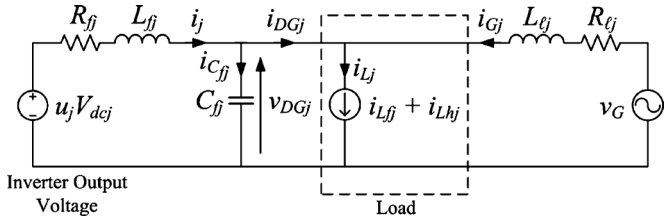

Fig. 4. Equivalent single-phase representation of the DG inverter of MT ($j = 1$) or PV array ($j = 2$) during grid-connected operation.

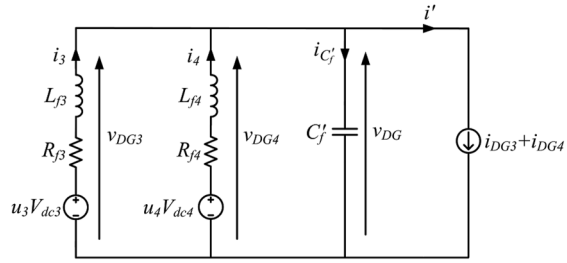

Fig. 5. Equivalent single-phase representation of the DG inverters of the SB ($j = 3$) and the PEMFC stack ($j = 4$) during islanded operation.

The load current i_{Lj}, where $j = 1, 2$, is modeled by two components consisting of fundamental i_{Lfj} and harmonic i_{Lhj} with their peak amplitudes I_{Lfj} and I_{Lhj}, respectively, and is represented by

$$\begin{aligned} i_{Lj} &= i_{Lfj} + i_{Lhj} = I_{Lfj}\sin(\omega t - \varphi_{Lfj}) \\ &\quad + \sum_{h=3,5,\ldots}^{N} I_{Lhj}\sin(h\omega t - \varphi_{Lhj}) \\ &= I_{Lfj}\sin\omega t\cos\varphi_{Lfj} - I_{Lfj}\cos\omega t\sin\varphi_{Lfj} \\ &\quad + \sum_{h=3,5,\ldots}^{N} I_{Lhj}\sin(h\omega t - \varphi_{Lhj}) \\ &= i_{Lfj,p} + i_{Lfj,q} + i_{Lhj} \end{aligned} \tag{4}$$

where φ_{Lfj} and φ_{Lhj} are the respective phase angles of the fundamental and harmonic components of i_{Lj} with respect to the distribution grid voltage v_G, and $i_{Lf,pj}$ and $i_{Lfj,q}$ are the instantaneous fundamental phase and quadrature components of i_{Lfj}. To achieve unity power factor at the PCC, compensate for the harmonics in the load currents and concurrently achieve load sharing, the DG inverter of the MT or PV array supplies a current $i_{\rm DG}$ given by

$$i_{\mathrm{DG}j} = (i_{Lfj,p} - i_{Gj}) + i_{Lfj,q} + i_{Lhj} \tag{5}$$

where $\mathrm{i}_{Gj}(j = 1, 2)$ is the grid current from the PCC.

As shown in Fig. 4, the distribution grid is supplied by a utility substation represented by a voltage source v_G during grid-connected operation and is connected to the microgrid and the load via a distribution line with resistance $R_{\ell j}$ and inductance $\mathrm{L}_{\ell j}$. In the grid-connected mode, the grid voltage is known, and the microgrid shares the load demand with the distribution grid. Hence, to control the power delivered to the load, the output current of the DG inverter of the MT or the PV array is regulated using the current control mode (CCM).

To derive a state-space model for the DG inverters during both grid-connected and islanded operations, Kirchhoff's

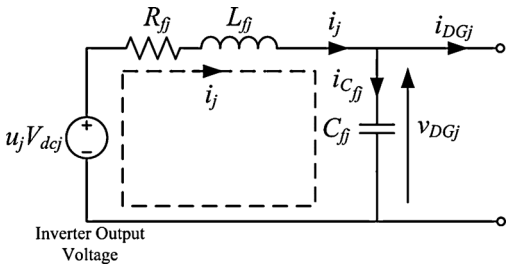

Fig. 6. Single-phase representation of the DG inverter during both grid-connected and islanded operations.

voltage and current laws are applied to the current loop i_j as shown in Fig. 6, and the following equations are obtained:

$$\frac{di_j}{dt} = -\frac{R_{fj}}{L_{fj}} i_j - \frac{1}{L_{fj}} v_{\mathrm{DG}j} + \frac{V_{dc}}{L_{fj}} u_j \tag{6}$$

$$\frac{dv_{\mathrm{DG}j}}{dt} = \frac{1}{C_{fj}} i_j - \frac{1}{C_{fj}} i_{\mathrm{DG}j} \tag{7}$$

where i_j is the current passing through L_{fj}. Hence, the grid-connected DG inverter model can be written as

$$\dot{x}_{gj} = A_{gj} x_{gj} + B_{gj1} v'_j + B_{gj2} u_j \tag{8}$$

$$y_{gj} = C_{gj} x_{gj} + D_{gj1} v'_j + D_{gj2} u_j \tag{9}$$

where the subscripts g and j represent the model of the DG inverter j during grid-connected operation ($j = 1, 2$) and

$$A_{gj} = -\frac{R_{fj}}{L_{fj}};\ B_{gj1} = \begin{bmatrix} -\frac{1}{L_{fj}} & 0 \end{bmatrix};\ B_{gj2} = \frac{V_{dcj}}{L_{fj}};$$
$$C_{gj} = 1;\ D_{gj1} = \begin{bmatrix} 0 & -C_{fj} \end{bmatrix};\ D_{gj2} = 0.$$

$x_{gj} = i_j$ is the state; $v'_j = \begin{bmatrix} v_{\mathrm{DG}j} & \frac{dv_{\mathrm{DG}j}}{dt} \end{bmatrix}^T$ is the exogenous input; u_j is the control input, with $-1 \le u_j \le 1$; and $y_{gj} = i_{\mathrm{DG}j}$ is the output, which will be regulated to track the desired periodic reference waveform. In our simulations to be presented in Section IV, DG inverters 3 and 4 are not in use during grid-connected operation but if they were, the same model could apply with $v_{\mathrm{DG3}} = v_{\mathrm{DG4}} = v_G$.

During islanded operation as shown in Fig. 5, the microgrid will supply the overall load demand. The voltage at the PCC needs to be regulated to a pure sine wave through the voltage control mode (VCM) with a desired magnitude and frequency generated by the droop controller. A state-space model for the DG inverters of the SB and the PEMFC stack can be derived similarly to obtain

$$\dot{x}_i = A_i x_i + B_{i1} i' + B_{i2} u \tag{10}$$

where the subscript i denotes islanded operation and

$$A_i = \begin{bmatrix} -\frac{R_{f3}}{L_{f3}} & 0 & -\frac{1}{L_{f3}} \\ 0 & -\frac{R_{f4}}{L_{f4}} & \frac{1}{L_{f4}} \\ \frac{1}{C'_f} & \frac{1}{C'_f} & 0 \end{bmatrix};\ B_{i1} = \begin{bmatrix} 0 \\ 0 \\ -\frac{1}{C'_f} \end{bmatrix}$$

$$B_{i2} = \begin{bmatrix} \frac{V_{dc3}}{L_{f3}} & 0 \\ 0 & \frac{V_{dc4}}{L_{f4}} \\ 0 & 0 \end{bmatrix}$$

with $C'_f = C_{f3} + C_{f4}$; $x_i = [\, i_3 \quad i_4 \quad v_G \,]^T$; $i' = i_{\mathrm{DG3}} + i_{\mathrm{DG4}}$; $u = [\, u_3 \quad u_4 \,]^T$. Since $i_{\mathrm{DG3}} + i_{\mathrm{DG4}} = i_{G1} + i_{G2}$ and $i_{Gj} = i_{Lj} - i_{\mathrm{DG}j} (j = 1, 2)$, it follows from (7) that if the line impedances associated with DG inverters 1 and 2 can be neglected (and hence $v_{\mathrm{DG}j} = v_G$), all DG inverters during islanded operation can be modeled individually into a unified form

$$\dot{x}_{ij} = A_{ij} x_{ij} + B_{ij1} i'_j + B_{ij2} u_j \tag{11}$$

$$y_{ij} = C_{ij} x_{ij} + D_{ij1} i'_j + D_{ij2} u_j \tag{12}$$

where $j = 1, 2, 3, 4$ and

$$A_{ij} = \begin{bmatrix} -\frac{R_{fj}}{L_{fj}} & -\frac{1}{L_{fj}} \\ \frac{1}{C'_f} & 0 \end{bmatrix};\ B_{ij1} = \begin{bmatrix} 0 \\ -\frac{1}{C'_f} \end{bmatrix};$$

$$B_{ij2} = \begin{bmatrix} \frac{V_{dcj}}{L_{fj}} \\ 0 \end{bmatrix}\ C_{ij} = \begin{bmatrix} 0 & 1 \\ 1 - \frac{C_{fj}}{C'_f} & 0 \end{bmatrix};$$

$$D_{ij1} = \begin{bmatrix} 0 \\ \frac{C_{fj}}{C'_f} \end{bmatrix};\ D_{gj2} = \begin{bmatrix} 0 \\ 0 \end{bmatrix}$$

with $C'_f = \sum_{n=1}^{4} C_{fn}$; $x_{ij} = [\, i_j \quad v_{\mathrm{DG}j} \,]^T$ is the state vector; $i'_j = \sum_m i_{Lm} - \sum_{n \neq j} i_n$ is the exogenous input of the DG inverter j; u_j is the control input, with $-1 \le u_j \le 1$; and $y_{ij} = [\, v_{\mathrm{DG}j} \quad i_{\mathrm{DG}j} \,]^T$ is the output, which will be regulated to track the desired reference waveform. Note that although the emphasis is on the voltage $\mathrm{v_{DG}}j$, both $v_{\mathrm{DG}j}$ and $i_{\mathrm{DG}j}$ will be regulated in the VCM to ensure the power delivered. Furthermore, it is assumed that the exogenous input i'_j in the model is not directly measurable by the DG inverter j since it involves quantities outside that inverter. Precisely, i'_j represents the sum of all load currents i_{Lm} minus the sum of all i_n from the other DG inverters $n \neq j$ in the microgrid. However, the information about i'_j can be derived using a Kalman filter applied to the output $y_{ij} = [\, v_{\mathrm{DG}j} \quad i_{\mathrm{DG}j} \,]^T$. The details are presented in Section III.

D. Droop Control for Parallel Operation of Inverters

The CB opens to isolate the microgrid from the distribution grid due to a fault on the upstream network of the distribution grid. As a result, the DG units in Fig. 1 are now the sole power sources left to supply the loads. The DG units will share the real and reactive power demand ΔP and ΔQ, respectively, such that in a microgrid with n DG inverters, we have

$$\Delta P = \sum_{j=1}^{n} \Delta P_j \tag{13}$$

$$\Delta Q = \sum_{j=1}^{n} \Delta Q_j \tag{14}$$

where ΔP_j and ΔQ_j are the real and reactive power variations of the jth DG inverter.

The sharing of the real and reactive power is achieved through the droop control method [7], [8] by regulating the magnitude and frequency of $v_{\mathrm{DG}j}$ when the jth DG inverter operates in the VCM, as described by the following equations:

$$\omega_j = \omega_{\mathrm{ref}} - k_{P,j} \times (P_{\mathrm{ref},j} - P_j) \tag{15}$$

$$v_{\mathrm{DG}j} = v_{\mathrm{ref}} - k_{Q,j} \times (Q_{\mathrm{ref},j} - Q_j) \tag{16}$$

where P_j and Q_j are the actual active and reactive power outputs of the jth DG unit, $k_{P,j}$ and $k_{Q,j}$ are the droop slopes (positive quantities) of the jth DG unit, ω_j and $v_{\mathrm{DG}j}$ are the actual operating frequency and output voltage of the jth DG unit, $P_{\mathrm{ref},j}$ and $Q_{\mathrm{ref},j}$ are the desired operating values usually selected based on the DG unit's power rating, and ω_{ref} and v_{ref} are the reference frequency and voltage magnitude when the microgrid operates in the islanded mode.

III. Model Predictive Control Design of DG Inverters

There have been some research works on the implementation of MPC for control of inverters. In [15], a Finite Control Set Model Predictive Control scheme which allows for the control of different converters without the need of additional modulation techniques or internal cascade control loops is presented but the research does not consider parallel operation of power converters. In [16], an investigation on the usefulness of the MPC in the control of parallel-connected inverters is conducted. The research is, however, focused mainly on the control of inverters for uninterruptible power supplies in stand-alone operation. There have been, however, limited research works on the implementation of MPC for parallel operation of DG inverters in a microgrid.

With the mathematical model developed in Section II, a novel MPC algorithm for the control of the DG inverters is proposed in this paper. The proposed controller is a newly developed MPC algorithm that decomposes the MPC optimization into two subproblems: a steady-state subproblem and a transient subproblem. Both problems can be solved in parallel in a receding horizon fashion to deal with grid-connected and islanded operations of the proposed microgrid. The decomposition of the control problem greatly reduces the computational burden and is designed specifically for fast-sampling systems to track periodic signals.

When the microgrid operates either connected or islanded from the distribution grid, the state-space model of the DG inverters after time-discretization will have the form

$$x^+ = Ax + B_1 w + B_2 u \tag{17}$$

$$y = Cx + D_1 w + D_2 u \tag{18}$$

where the superscript $+$ denotes the time-shift operator (with a sampling interval of T_s), and w is the periodic exogenous signal. Generally, for any periodic signal that has a finite number of harmonics, the signal can be expressed as the output of an autonomous finite-dimensional LTI state-space model. For example, if the periodic signal has a fundamental frequency ω and consists of only odd harmonics, the A -matrix of the corresponding state-space model can be expressed in a block diagonal form given by

$$\begin{bmatrix} \cos(h\omega T_s) & \sin(h\omega T_s) \\ -\sin(h\omega T_s) & \cos(h\omega T_s) \end{bmatrix}$$

where $h = 1, 3, 5, \ldots$, and the C-matrix is given by $[1 \;\; 0 \;\; 1 \;\; 0 \;\; \ldots \;\; 1 \;\; 0]$. Furthermore, the magnitude and phase angle of this periodic signal can be determined by the initial state of this autonomous model. Hence, the exogenous signal w in (17) and (18) and the reference d, which is required to be tracked by y in (18), can be modeled by

$$\xi^+ = A_\xi \xi \tag{19}$$

$$w = C_w \xi \tag{20}$$

$$d = C_d \xi \tag{21}$$

for some A_ξ, C_w, and C_d as described above. During grid-connected operation, the DG inverter of the MT or PV array operates in the CCM, the output y and the reference d that i_{DG} is required to track should typically consist of the same order of harmonics as i_L (otherwise some harmonics of i_L will be able to enter the distribution grid unregulated) and is derived from the desired active and reactive power outputs of the DG unit. However, during islanded operation, the DG inverters of the SB and the PEMFC stack operate in the VCM. In addition, $y = [\, v_{\mathrm{DG}} \quad i_{\mathrm{DG}} \,]^T$ for the DG units, and the first component of the reference d, which is required to be tracked by v_{DG}, is typically a pure sine wave, and its frequency and magnitude can be defined by (13) and (14), respectively.

The state-space model in (19)–(21) is known as the exogenous system in this paper. Although only odd harmonics up to the 29th order have been considered in this paper, the proposed methodology can be readily extended to include even harmonics and higher order harmonics. The exogenous state ξ, which essentially represents the sets of the Fourier coefficients of w and d, can be automatically identified using a Kalman-based observer. During islanded operation, w is not directly measurable but the exogenous system can be combined with the DG inverter model (11)–(12) so that the observer can be applied via the measurement of y and the known d.

In this paper, a sampling interval of $T_s = 0.2$ ms has been selected for the simulation studies. This selected interval is considered pretty fast in conventional MPC applications, but is necessary for the present control problem due to the high order of harmonics being tackled. With state-of-the-art code generation techniques, sampling in the range of tens of kHz is possible [17].

The control signal u in (17) and (18) is decomposed into a steady-state control u_s and a transient control u_t as follows:

$$u = u_s + u_t \tag{22}$$

such that $u \to u_s$ and $u_t \to 0$ asymptotically. Both u_s and u_t will employ an MPC strategy, but the former will adopt a dynamic MPC policy, whereas the latter will adopt a more conventional finite-horizon approach. The approaches adopted for the two subproblems are different because the conventional finite-horizon approach requires a very long horizon to solve a steady-state subproblem, which makes it computationally intensive. Through decomposition, the solution to the steady-state subproblem can be computed using a different method that will trade the best possible performance for a lower complexity. Hence, a much smaller T_s can be selected to produce a fast-sampling control system that would otherwise be impossible. The detailed mathematical formulations of the control designs for the steady-state and transient subproblems will be presented in the following subsections.

A. Steady-State Subproblem

In the steady-state subproblem, $x \to x_s, y \to y_s$ and $u \to u_s$ asymptotically. Based on (17) and (18), u_s, x_s, and y_s should obviously satisfy

$$x_s^+ = Ax_s + B_1 w + B_2 u_s \tag{23}$$

$$y_s = Cx_s + D_1 w + D_2 u_s \tag{24}$$

subject to the constraint

$$|u_s| \leq 1. \tag{25}$$

Ideally, y_s is required to be equal to the desired reference d, or equivalently, the asymptotic tracking error

$$e_s = y_s - d = 0. \tag{26}$$

However, this situation is not always possible due to the constraint given by (25). Considering the steady-state control u_s being generated from a dynamic MPC policy

$$\hat{\xi}^+ = A_{\hat{\xi}}\hat{\xi} \tag{27}$$

$$u_s = C_{\hat{\xi}}\hat{\xi} \tag{28}$$

where the matrices $A_{\hat{\xi}}$ and $C_{\hat{\xi}}$ are designed offline, but the initial state $\hat{\xi}$ at time k will be optimized online in a receding horizon fashion. Hence, x_s can be written as a linear function of the exogenous state ξ and the controller state $\hat{\xi}$ as follows:

$$x_s = X\xi + \hat{X}\hat{\xi} \tag{29}$$

where the matrices X and $\hat{X}$ satisfy

$$XA_\xi = AX + B_1C_w \tag{30}$$

$$\hat{X}A_{\hat{\xi}} = A\hat{X} + B_2C_{\hat{\xi}}. \tag{31}$$

Furthermore, both y_s and e_s are linear functions of ξ and $\hat{\xi}$ as follows:

$$\begin{aligned} y_s &= Cx_s + D_1w + D_2u_s \\ &= (CX + D_1C_w)\xi + (C\hat{X} + D_2C_{\hat{\xi}})\hat{\xi} \end{aligned} \tag{32}$$

$$\begin{aligned} e_s &= y_s - d \\ &= y_s - C_d\xi \\ &= (CX + D_1C_w - C_d)\xi + (C\hat{X} + D_2C_{\hat{\xi}})\hat{\xi}. \end{aligned} \tag{33}$$

With the estimation of the exogenous state ξ provided online by the Kalman filter, the optimization problem

$$\begin{aligned} &\min_{\hat{\xi}(k)} \sum_i e_s(k+i)^T Q e_s(k+i) \\ &\quad \text{subject to } |u_s(k+i)| \leq 1 \end{aligned} \tag{34}$$

can then be solved to obtain the optimal controller state $\hat{\xi}(k)$ and accordingly the steady-state control $u_s(k)$, where the sum in (34) is carried out over one "nominal" period of 0.02 s, and Q is a given positive definite matrix. The dynamic models (27) and (28) provide a projection or prediction model of the future u_s, whereas the actual future u_s will be recomputed from (34) as the horizon moves forward (the so-called "receding horizon" approach). The controller dynamics $A_{\hat{\xi}}$ and $C_{\hat{\xi}}$ can be constructed to meet the following conditions:

1) Systems (27) and (28) are observable.
2) $A_{\hat{\xi}}$ consists of the same order of harmonics as A_ξ in (19).
3) A transformation matrix T (need not be a square matrix) exists, such that $\hat{\xi} = T\xi$ for all time and it also results in $e_s = 0$. In other words, the unconstrained optimization

$$\min_{\hat{\xi}(k)} \sum_i e_s(k+i)^T Q e_s(k+i) \tag{35}$$

will have a zero value at $\hat{\xi}(k) = T\xi(k)$.

These conditions will guarantee that the MPC optimization will have a unique optimizer $\hat{\xi}(k)$, and the dynamic control laws (27) and (28) are equivalent to the optimal state-feedback law given by $u_s = C_{\hat{\xi}}T\xi$ as long as the constraint $|u_s| \leq 1$ is not violated.

B. Transient Subproblem

To solve the transient subproblem, the transient signals $u_t = u - u_s, x_t = x - x_s$ and $y_t = y - y_s$ are defined. Based on (17), (18), (23), and (24), u_t, x_t, and y_t should satisfy

$$x_t^+ = Ax_t + B_2u_t \tag{36}$$

$$y_t = Cx_t + D_2u_t. \tag{37}$$

The objective of this transient subproblem is to make $y_t \to 0$ as fast as possible, subject to the constraint

$$|u_s + u_t| \leq 1. \tag{38}$$

To solve the transient subproblem, a more conventional MPC approach that employs a finite horizon with a terminal cost can be adopted. More precisely, for the given positive definite matrices Q and R and the chosen length of control horizon N_u, we solve

$$\begin{aligned} &\min_{u(k+i)} \sum_{i=1}^{N_u} (y_t(k+i)^T Q y_t(k+i) \\ &\quad + u_t(k+i)^T R u_t(k+i)) \\ &\quad + x_t(N_u+1)^T P_T x_t(N_u+1) \\ &\text{subject to } |u_s(k+i) + u_t(k+i)| \leq 1. \end{aligned} \tag{39}$$

The matrix A in the present case is stable. Hence, an appropriate choice of P_T is the weighted observability gramian obtained from the Lyapunov equation

$$A^T P_T A - P_T + C^T Q C = 0 \tag{40}$$

which makes the optimization in (39) equivalent to

$$\begin{aligned} &\min_{u(k+i)} \sum_{i=1}^{\infty} (y_t(k+i)^T Q y_t(k+i) \\ &\quad + u_t(k+i)^T R u_t(k+i)) \\ &\quad \text{subject to} \\ &\quad |u_s(k+i) + u_t(k+i)| \leq 1 \text{ for } i \leq N_u \\ &\quad \text{and } u_t(k+i) = 0 \text{ for } i > N_u. \end{aligned} \tag{41}$$

The optimization given by (41) requires the information of u_s and x_s, which are provided by the solution of the steady-state subproblem, and the information of the plant state x, which can be estimated using a plant Kalman filter on (17) and (18). The overall configuration of the proposed control strategy combining the steady-state control signal u_s and the transient control signal u_t is shown in Fig. 7. As for the horizon lengths, the control and prediction horizons of the transient MPC are both 10 with a properly chosen terminal cost. The steady-state MPC is a dynamic MPC policy and therefore does not have a control horizon as in the conventional MPC. However, the number of constraints depends on the prediction horizon which is 50, corresponding to half of the fundamental period ($50 \times 0.2\,\text{ms} = 0.01$ s). As mentioned above, the task of the steady-state MPC is to generate the optimal voltage and current references and it can be updated at a lower rate if necessary.

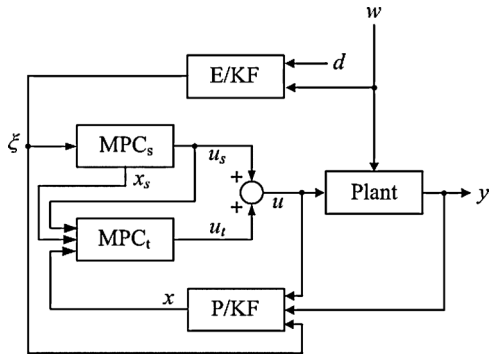

Fig. 7. Overall MPC controller for the DG inverter with E/KF denoting the exogenous Kalman filter and P/KF denoting the plant Kalman filter.

TABLE I
PARAMETERS OF THE PROPOSED SYSTEM

Parameter	Value
Distribution grid voltage	v_G = 230Vrms (phase)
DC link voltage	V_{dc} = 400Vdc
Distribution line impedance	R_ℓ = 7.5mΩ, L_ℓ = 25.7μH
Transformer impedance	R_T = 1.9mΩ, L_T = 28.6μH
LC filter	L_f = 1.2mH, C_f = 20μF
DG inverter loss resistance	R_f = 0.01Ω

IV. SIMULATION STUDIES

The simulation model of the microgrid shown in Fig. 1 is realized in Matlab/Simulink. The microgrid is tested under different simulation scenarios to evaluate its capabilities when operating connected and islanded from the distribution grid. Different load types consisting of linear and nonlinear loads are considered in the studies. Load 1 is characterized by a three-phase dimmer load with real and reactive power demand of $P_{L,1} = 15$ kW and $Q_{L,1} = 9.7$ kVAr. The dimmer load is modeled as a current source with its harmonic contents determined through experimental results obtained from several light dimmers in [18]. Load 2 is a three-phase RL load with real and reactive power demand of $P_{L,2} = 5$ kW and $Q_{L,2} = 3$ kVAr. The system parameters are given in Table I. The impedances of the distribution lines and the transformer have been obtained based on the details presented in [19]. The DG inverter loss resistance has been coarsely estimated because it is not precisely known in practice.

A. Test Case 1: Power Quality Improvement With Load Sharing During Grid-Connected Operation

During grid-connected operation, the main DG units are required to provide power for the loads to reduce the burden of generation and delivery of power directly from the distribution grid. The first test case demonstrates how the power flows are managed among the distribution grid, the DG units, and the loads. In this test case, DG inverter 1 of the MT DG unit is tasked to provide 50% of $P_{L,1}$, and DG inverter 2 of the PV DG unit delivers 60% of $P_{L,2}$. The rest of the real power demand of Loads 1 and 2 are supplied by the grid. The SB is operating in the charge mode to store energy during off-peak period where the cost of generation from the grid is cheaper to meet future sudden demands for power, whereas the PEMFC stack is in the idle mode. The first test case also demonstrates the capability of the DG units to improve the power quality of the distribution network by compensating for the harmonics in the load current. In this test case, DG inverter 1 is controlled to compensate for the harmonic current of Load 1 due to the nonlinear three-phase dimmer load connected to the MT DG unit. In this way, the harmonics will not propagate to the rest of the distribution network during grid-connected operation.

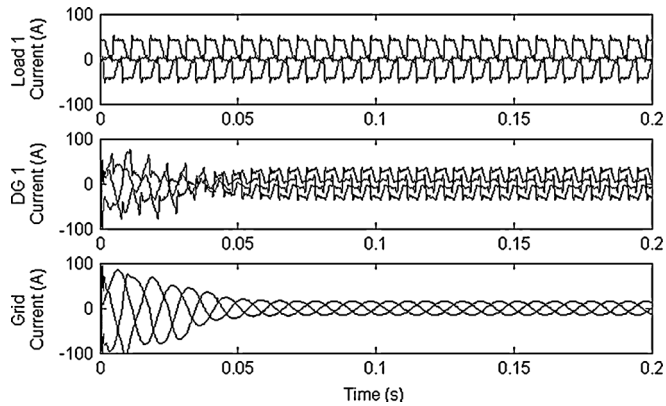

Fig. 8. Waveforms of three-phase load 1 current i_{L1} (top), three-phase DG 1 current i_{DG1} (middle), and three-phase grid current i_{G1} (bottom).

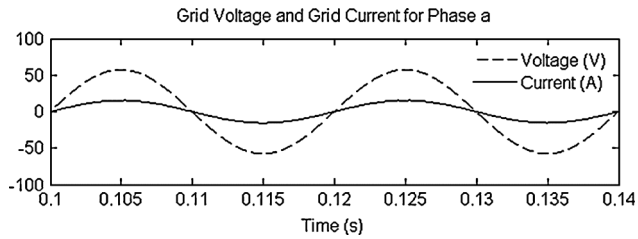

Fig. 9. Waveforms of grid voltage v_G and grid current i_{G1} for phase a.

The waveforms of the current delivered to Load 1 by the distribution grid at the PCC i_{G1}, the current supplied by DG inverter 1 i_{DG1}, and the current delivered to Load 1 i_{L1} under this test case for $0 \leq \mathrm{t} < 0.2$ s are shown in Fig. 8. The unsteady measurement in i_{G1} during the initialization for $0 \leq \mathrm{t} < 0.06$ s shown in Fig. 8 (bottom) is due to the fact that the controller needs a period of 3 cycles to track the generated references. During the initialization, large current transients are also observed in i_{DG1} as shown in Fig. 8 (middle). In our simulation studies, it is assumed that with the current technology in the development of power electronic devices, the inverter will be able to withstand such large transients. During steady-state condition, the total harmonic distortion (THD) value of i_{L1} is 41.7%, as shown in Fig. 8 (top). With DG inverter 1 supplying the harmonic current of Load 1, as shown in Fig. 8 (middle), the THD value of i_{G1} is improved to about 0.4%, as shown in Fig. 8 (bottom). To achieve power factor correction at the grid side, DG inverter 1 is also controlled to provide the reactive component $i_{Lf1,q}$ of the current i_{L1}, as given in (5). Fig. 9 shows the closed-up waveforms of the grid voltage v_G (the voltage has been scaled down by a factor of 0.25 for comparison) and grid current i_{G1} of phase a for $0.1 \leq \mathrm{t} < 0.14$ s. As observed, the waveform of i_{G1} is in phase with that of v_G with power factor correction.

The real and reactive powers dispatched by the DG inverters 1 and 2 for $0 \leq \mathrm{t} < 0.2$ s are shown in Figs. 10 and 11, respectively. The real powers dispatched by DG inverters 1 and

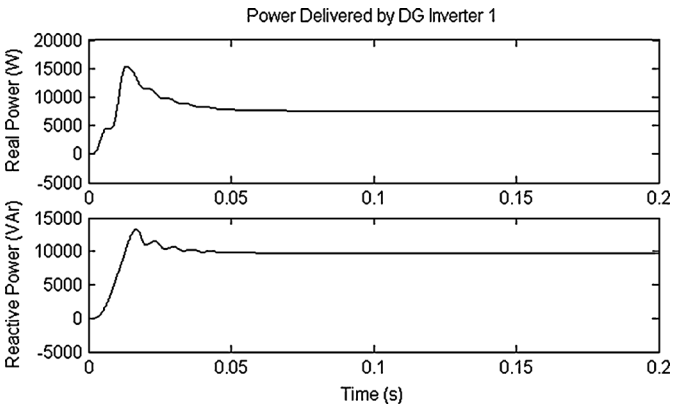

Fig. 10. Real (top) and reactive (bottom) power delivered by DG inverter 1.

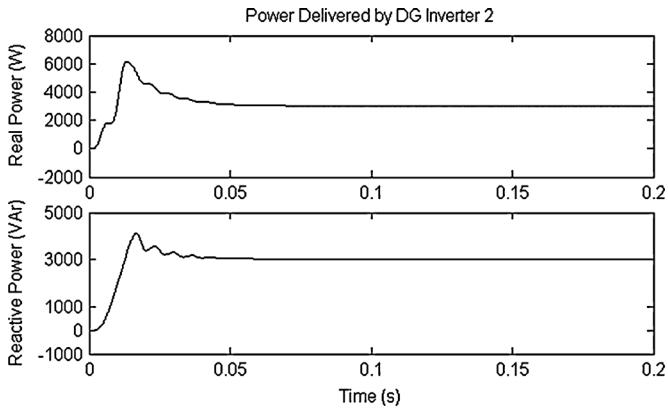

Fig. 11. Real (top) and reactive (bottom) power delivered by DG inverter 2.

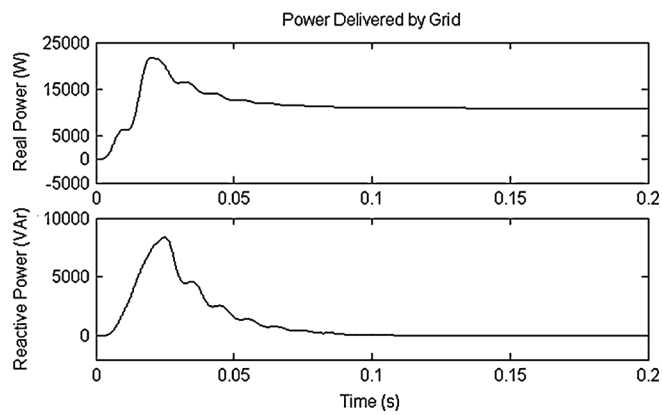

Fig. 12. Total real (top) and reactive (bottom) power delivered by the grid to loads 1 and 2, and to charge the SB.

2 are 7.5 kW (50% of $P_{L,1}$) and 3 kW (60% of $P_{L,2}$), respectively, as shown in Figs. 10 and 11. The real powers dispatched by both inverters demonstrate the capability of the DG units to dispatch the required power. The DG units also deliver all the reactive power of 12.7 kVAr required by the loads to achieve unity power factor at the grid side. The total real and reactive power delivered by the grid to Loads 1 and 2, and to charge up the SB for $0 \leq \mathrm{t} < 0.2$ s is shown in Fig. 12. As shown in Fig. 12, the grid supplies 7.5 kW (50% of $P_{L,1}$) and 2 kW (40% of $P_{L,2}$), and also dispatches an additional power of about 1.5 kW to charge the SB. In addition, the reactive power supplied by the grid is zero, which results in unity power factor at the grid side.

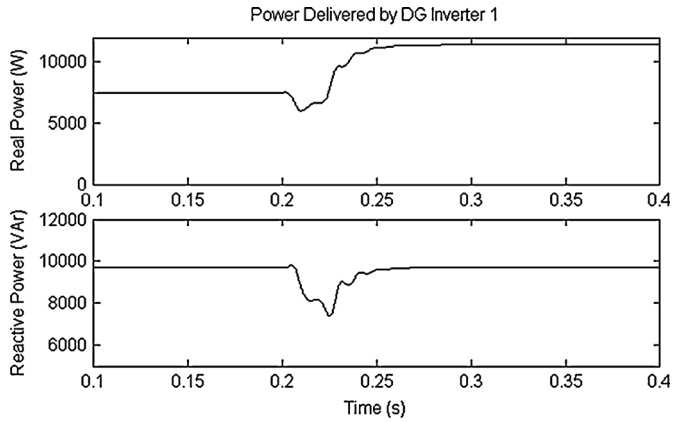

Fig. 13. Real (top) and reactive (bottom) power delivered by DG inverter 1.

B. Test Case 2: Load Sharing During Islanded Operation With Droop Control

The second test case demonstrates the sharing of real and reactive power among the back-up DG units, i.e., the SB and the PEMFC stack when the microgrid transits to islanded operation. In this test case, the microgrid is operating in the grid connected operation for $0 \leq \mathrm{t} < 0.2$ s. At $\mathrm{t} = 0.2$ s, a fault occurs on the upstream network of the distribution grid, and the CB operates to disconnect the microgrid from the distribution grid.

The real and reactive power delivered by DG inverter 1 for $0.1 \leq \mathrm{t} < 0.4$ s is shown in Fig. 13. As shown in Fig. 13, the MT DG unit increases its generation to about 11.4 kW to supply $P_{L,1}$ for $0.2 \leq \mathrm{t} < 0.4$ s. The reactive power delivered by the MT remains constant at 9.7 kVAr as in test case 1. The real and reactive power delivered by DG inverter 2 for $0.1 \leq \mathrm{t} < 0.4$ s is shown in Fig. 14. As shown in Fig. 14, the real and reactive power delivered by the PV array remains constant at 3 kW and 3 kVAr, respectively. The generation of the MT and the PV DG units are unable to meet the overall power demand of Loads 1 and 2 when the microgrid islands itself from the grid. Therefore, the SB and the PEMFC stack are required to share the load demand. The automatic sharing of this load demand can be achieved using the frequency and voltage droop control method discussed in Section II-D. As in the previous test cases, the MT and the PV array are controlled by the inverters to supply the reactive power demands of 9.7 kVAr and 3 kVAr of Loads 1 and 2, respectively. Hence the back-up DG units are required to provide only for the real power demand because network cable impedances do not allow a precise sharing of reactive power among the DG inverters [4], [7], [8]. Without the need to deliver reactive power, the power loss in the distribution lines is also reduced.

The real power outputs of DG inverters 3 and 4 of the SB and the PEMFC stack for $0.1 \leq \mathrm{t} < 0.4$ s are shown in Figs. 15 and 16, respectively. Both the SB and the PEMFC stack are in the idle mode for $0 \leq \mathrm{t} < 0.2$ s. After the initiation of the islanding operation at $\mathrm{t} = 0.2$ s, DG inverters 3 and 4 increase their generation to provide real powers of about 3.28 kW and 2.28 kW to the loads, which reach steady-state operation in about 0.5 cycle. The waveform of v_{DG} for $0.1 \leq \mathrm{t} < 0.4$ s is also shown in Fig. 17. During islanded operation, the operating frequency

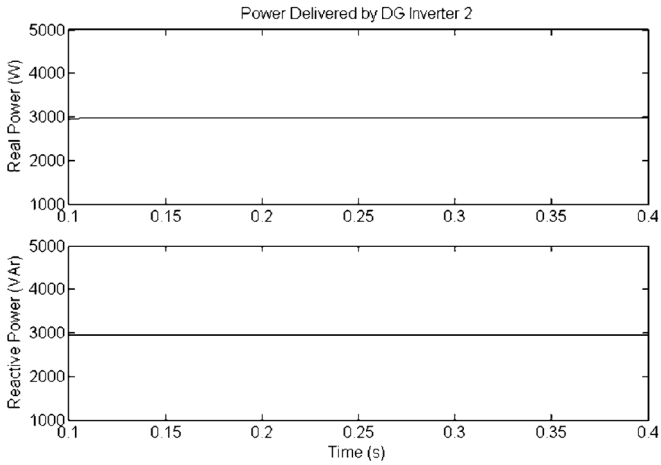

Fig. 14. Real (top) and reactive (bottom) power delivered by DG inverter 2.

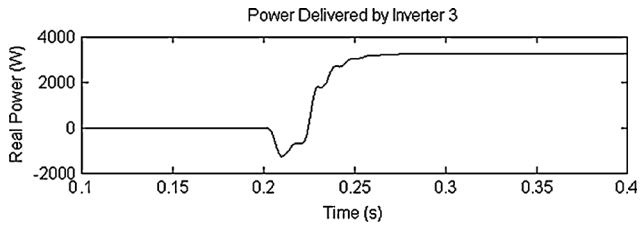

Fig. 15. Real power delivered by DG inverter 3.

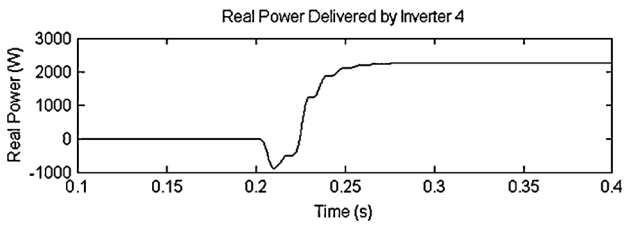

Fig. 16. Real power delivered by DG inverter 4.

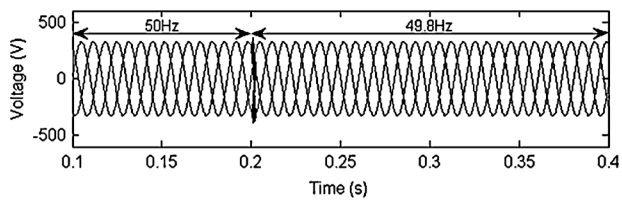

Fig. 17. Inverter output voltage v_{DG} of DG units 3 and 4.

of v_{DG} is reduced from 50 Hz (prior to islanding) to about 49.8 Hz for $0.2 \leq \mathrm{t} < 0.4$ s.

C. Test Case 3: Investigation on Network Voltage Changes

In Singapore, distribution system operators are obliged to supply their customers a voltage within $\pm 6\%$ of the nominal voltage at the low-voltage distribution network. As shown in Fig. 1, various DG units are connected directly to the PCC. Hence the flow of real and reactive power within the microgrid can change, which consequently changes the voltage profile for any loads that are connected to the PCC when the microgrid operates in the islanded mode. This change in voltage ΔV due to the DG units delivering real and reactive power can be given by

$$\Delta V = \frac{PR + QX}{V} \tag{42}$$

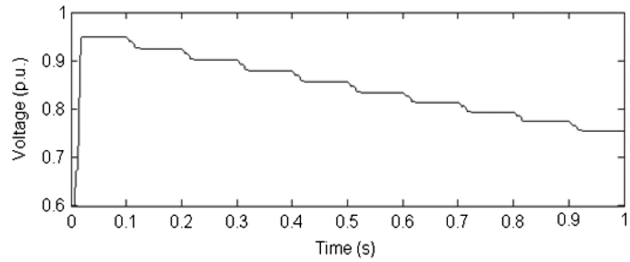

Fig. 18. Voltage profile (in p.u.) for changes in the real and reactive power of the load demand.

where R and X are the resistance and reactance of the distribution line, and V is the voltage at the load side. From (42), both the distribution line resistance and reactance have a significant effect on the voltage profile at the load side as compared with the transmission network where the lines are assumed to be mainly inductive [20].

The third test case investigates the changes in the network voltage when loads with different power demands are being connected to the PCC during islanded operation of the microgrid. In this test case, a load with an initial real and reactive power demand of 2 kW and 1.24 kVAr, respectively, is connected to the PCC of the microgrid as shown in Fig. 1. To investigate the effect of the real and reactive power demand of the load on the PCC voltage, the real and reactive power demand of the load is increased in a step-size of 1 kW and 0.62 kVAr every 0.1 s, such that the power factor of the load is maintained at a constant value of about 0.85. The waveform of the voltage profile (in per unit (p.u.) value) for incremental changes in the real and reactive power of the load demand for $0 \leq \mathrm{t} < 1$ s is shown in Fig. 18. As shown in Fig. 18, the increments in the real and reactive power demand of the load cause a significant drop in the PCC voltage, as given by (42). The initial PCC voltage is about 0.96 p.u. under the initial load demand. However, with the increment of load demand, the PCC voltage drops to about 0.75 p.u. Hence it can be concluded that as the real and reactive power demand by the load increases, the voltage drop will increase. To overcome the problem caused by the effect of loading connected to the PCC, several methods can be implemented. One conventional technique is to integrate a tap-changing transformer to regulate the voltage received by the customers such that the voltage is allowed to vary within the allowable range of $\pm 6\%$ under different loading conditions [9].

D. Test Case 4: Investigation on Increased Fault Level

The integration of DG units into the low-voltage distribution network will lead to a more complex flow of fault currents for any fault occurring in the microgrid. These DG units, connected to the microgrid through interfacing voltage source inverters, will alter the fault level of the low-voltage distribution network. The fourth test case investigates how the integration of DG units into the existing distribution network will contribute to the network fault level, which will in turn affect the operation of the existing CBs and the distribution cables.

The test case is characterized by the scenario when a fault occurs on the line that is connected to the MT DG unit (point F) as shown in Fig. 1, which will result in the flow of fault currents from the MT DG unit, the PV DG unit, and the distribution grid, thus increasing the fault level at the CB connected to the line of the MT DG unit. Fig. 19 shows the equivalent single-line

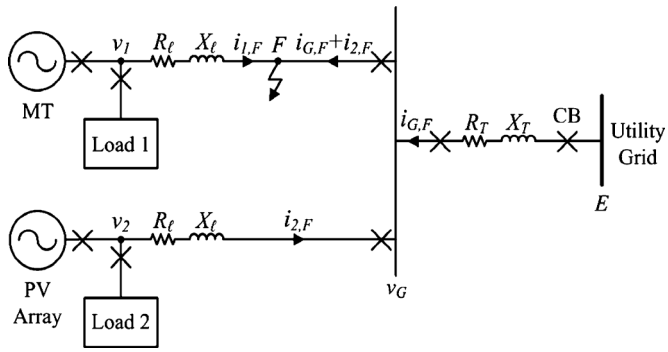

Fig. 19. Equivalent single-line diagram of the proposed microgrid during fault analysis.

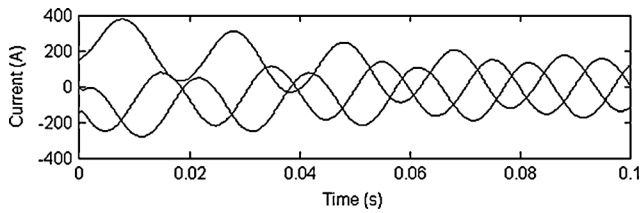

Fig. 20. Fault current from DG inverter 1.

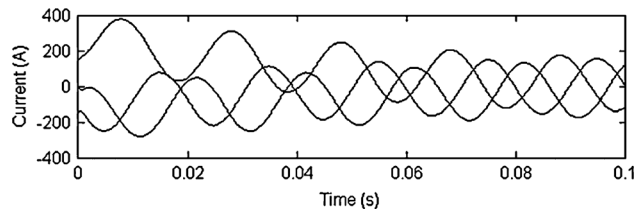

Fig. 21. Fault current from DG inverter 2.

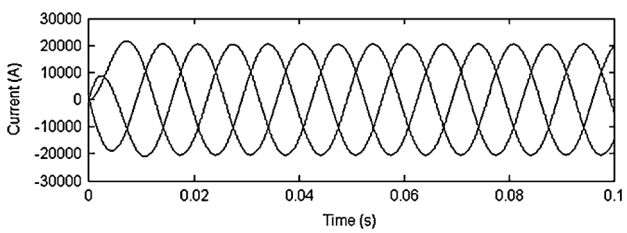

Fig. 22. Fault current from distribution grid.

diagram of the proposed microgrid in Fig. 1 in this test case. Table II summarizes the numerical values of the currents and voltages at different points of the distribution network during the fault at point F. The waveforms of the fault currents from DG units 1 and 2, and the grid for $0 < t < 0.1$ s are also shown in Figs. 20, 21, and 22 respectively. The DG inverters can provide only a small amount of short circuit current, which usually ranges from 1.5 p.u. to 2 p.u. depending on the ratings of the inverters [7], [9]. In this test case, the fault current contributed by DG inverters 1 and 2 is restricted to 2 p.u. Hence, the integration of the MT and the PV DG units into the distribution grid increases the fault level at point F by about 2.69%.

One possible method to reduce the increased fault level caused by the increased penetration of DG units into the distribution network is to increase the short-circuit ratings of the existing CBs and the cables at the expense of greater costs. The implementation of this scheme would also be difficult, particularly in congested city substations and cable routes. The fault level contribution by the DG units may also be reduced by artificially introducing reactances between the DG units and the distribution network through a reactor.

TABLE II
NUMERICAL VALUES OF CURRENTS AND VOLTAGES DURING FAULT

Parameter	Value (p.u.)
Distribution grid voltage (high-voltage side)	$E = 1\angle 0.0402°$
Distribution grid voltage (low-voltage side)	$v_G = 1\angle 0°$
Output voltage of DG inverter 1	$v_1 = 0.9997\angle -0.0217°$
Output voltage of DG inverter 2	$v_2 = 0.9998\angle -0.0145°$
Fault current from distribution grid	$i_{G,F} = 251\angle -77.81°$
Fault current from DG inverter 1 (MT)	$i_{1,F} = 2\angle -47.14°$
Fault current from DG inverter 2 (PV array)	$i_{2,F} = 2\angle -47.13°$

V. CONCLUSION

In this paper, a centralized control system that coordinates parallel operation of multiple inverters in a microgrid for both grid-connected and islanded operations has been proposed. The controller of the DG inverters is designed to operate in two modes. When the microgrid operates connected to the grid, the controller is set to operate in the current control mode to control the real and reactive power delivered to the load. When the microgrid is operating islanded from the grid, the DG inverters operate in the voltage control mode to regulate the output voltages of the DG inverters. An energy management algorithm for the operation of the main DG units and the back-up DG units is also implemented when the microgrid operates in either the grid-connected or islanded mode. The proposed controller is based on a newly developed MPC algorithm that decomposes the control problem into steady-state and transient subproblems to reduce the overall time of computation. The controller also integrates Kalman filters into the control design to generate the necessary references for the controller. When the microgrid is operating islanded from the grid, the back-up DG units are controlled to share the power demand through the droop control method. The design concept has been tested under different simulation scenarios. The results obtained validate that the microgrid can handle different operating conditions effectively during grid-connected and islanded operations, thus increasing the overall reliability of the distribution system. The alteration of the voltage profiles and the fault levels in the distribution network caused by the increased penetration of DG units into the distribution grid has also been investigated using the proposed microgrid. However, the proposed design concept still needs further validation through experimental studies. The simulation results obtained in this paper and the analysis carried out serve as a fundamental step towards the design of control circuits for the future hardware implementation of the microgrid.

REFERENCES

[1] R. Lasseter, A. Akhil, C. Marnay, J. Stevens, J. Dagle, R. Guttromson, A. S. Meliopoulous, R. Yinger, and J. Eto, "Integration of distributed energy resources—The CERTS microgrid concept," prepared by: Lawrence Berkeley National Laboratory for California Energy Commission, White Paper, Oct. 2003 [Online]. Available: http://certs.lbl.gov/pdf/50829-app.pdf

[2] H. Nikkhajoei and R. Lasseter, "Distributed generation interface to the CERTS microgrid," *IEEE Trans. Power Del.*, vol. 24, no. 3, pp. 1598–1608, Jan. 2009.

[3] A. Chambers, S. Hamilton, and B. Schnoor, *Distributed Generation: A Nontechnical Guide*. Tulsa, OK: PennWell, 2001.
[4] A. Tuladhar, H. Jin, T. Unger, and K. Mauch, "Parallel operation of single phase inverter modules with no control interconnections," in *Proc. 12th Annu. Appl. Power Electron. Conf. Expo.*, 1997, vol. 1, pp. 94–100.
[5] K. De Brabandere, B. Bolsens, J. Van den Keybus, A. Woyte, and J. Driesen, "A voltage and frequency droop control method for parallel inverters," *IEEE Trans. Power Electron.*, vol. 22, no. 4, pp. 1107–1115, Jul. 2007.
[6] J. M. Guerrero, J. Matas, L. G. Vicuña, M. Castilla, and J. Miret, "Decentralized control for parallel operation of distributed generation inverters using resistive output impedance," *IEEE Trans. Ind. Electron.*, vol. 54, no. 2, pp. 994–1004, Apr. 2007.
[7] J. A. P. Lopes, C. L. Moreira, and A. G. Madureira, "Defining control strategies for microgrids islanded operation," *IEEE Trans. Power Syst.*, vol. 21, no. 2, pp. 916–924, May 2006.
[8] Y. Li, D. M. Vilathgamuwa, and P. Loh, "Design, analysis, and real-time testing of a controller for multibus microgrid system," *IEEE Trans. Power Electron.*, vol. 19, no. 5, pp. 1195–1204, Sep. 2004.
[9] N. Jenkins, J. Ekanayake, and G. Strbac, *Distributed Generation*. Stevenage, U.K.: Inst. Eng. Technol., 2009.
[10] C. L. Chen, Y. B. Wang, J. S. Lai, Y. S. Lai, and D. Martin, "Design of parallel inverters for smooth mode transfer of microgrid applications," *IEEE Trans. Ind. Electron.*, vol. 25, no. 1, pp. 6–15, Jan. 2010.
[11] M. Charkhgard and M. Farrokhi, "State-of-charge estimation for lithium-ion batteries using neural networks and EKF," *IEEE Trans. Ind. Electron.*, vol. 57, no. 12, pp. 4178–4187, Jun. 2010.
[12] M. Coleman, C. K. Lee, C. Zhu, and W. G. Hurley, "State-of-charge determination from EMF voltage estimation: Using impedance, terminal voltage, and current for lead-acid and lithium-ion batteries," *IEEE Trans. Ind. Electron.*, vol. 54, no. 5, pp. 2550–2557, Oct. 2007.
[13] W. X. Shen, C. C. Chan, E. W. C. Lo, and K. T. Chau, "Adaptive neuro-fuzzy modeling of battery residual capacity for electric vehicles," *IEEE Trans. Ind. Electron.*, vol. 49, no. 3, pp. 677–684, Jun. 2002.
[14] A. Gosh and G. Ledwich, *Power Quality Enhancement Using Custom Power Devices*. Norwell, MA: Kluwer, 2002, pp. 380–406.
[15] S. Kouro, P. Cortés, R. Vargas, U. Ammann, and J. Rodríguez, "Model predictive control—A simple and powerful method to control power converters," *IEEE Trans. Ind. Electron.*, vol. 56, no. 6, pp. 1826–1838, Jun. 2009.
[16] K. S. Low and R. Cao, "Model predictive control of parallel-connected inverters for uninterruptible power supplies," *IEEE Trans. Ind. Electron.*, vol. 55, no. 8, pp. 2884–2893, Aug. 2008.
[17] J. Mattingley, Y. Wang, and S. Boyd, "Receding horizon control: Automatic generation of high-speed solvers," *IEEE Control Syst. Mag.*, vol. 31, no. 3, pp. 52–65, Jun. 2011.
[18] K. H. Kwan, Y. C. Chu, and P. L. So, "Model-based H_∞ control of a unified power quality conditioner," *IEEE Trans. Ind. Electron.*, vol. 56, no. 7, pp. 2493–2504, Jul. 2009.
[19] C. Y. Teo, *Principles and Design of Low Voltage Systems*. Singapore: Byte Power Publ., 1997.
[20] C. L. Masters, "Voltage rise: The big issue when connecting embedded generation to long 11 kV overhead lines," *IET Power Eng. J.*, vol. 16, no. 1, pp. 5–12, 2002.

K. T. Tan (S'08) received the B.Eng. degree in electrical and electronic engineering from Nanyang Technological University, Singapore, in 2008, where he is currently working towards the Ph.D. degree in the Laboratory for Clean Energy Research, School of Electrical and Electronic Engineering.

His research interests include clean and renewable energy, microgrids, and smart grids.

X. Y. Peng (S'11) received the B.Eng. degree in electrical and electronic engineering from Wuhan University, China, in 2010 and the M.Sc. degree in power engineering from Nanyang Technological University, Singapore, in 2011. He is currently working toward the Ph.D. degree in the Laboratory for Clean Energy Research, School of Electrical and Electronic Engineering, Nanyang Technological University.

His research interests include smart grids, control strategy in microgrids, and distributed energy resources.

P. L. So (M'98–SM'03) received the B.Eng. degree with first class honors in electrical engineering from the University of Warwick, U.K., in 1993 and the Ph.D. degree in electrical power systems from Imperial College, University of London, U.K., in 1997.

He is currently an Associate Professor in the School of Electrical and Electronic Engineering, Nanyang Technological University, Singapore. Prior to his academic career, he worked for 11 years as a Second Engineer with China Light and Power Company Limited, Hong Kong, in the field of power system protection. His research interests are power system stability and control, power quality, power line communications, clean and renewable energy, as well as microgrids and smart grids.

Dr. So was the Chair of the IEEE Singapore Section from 2009 to 2010. Currently he is a Member of the Electrical Testing Technical Committee, Singapore Accreditation Council, and a Member of Working Group under the purview of the Telecommunications Standards Technical Committee, Infocomm Development Authority (iDA) of Singapore.

Y. C. Chu (S'88–M'97–SM'06) received the B.Sc. degree in electronics and the M.Phil. degree in information engineering from the Chinese University of Hong Kong, Hong Kong, in 1990 and 1992, respectively, and the Ph.D. degree in control from the University of Cambridge, Cambridge, U.K., in 1996.

He then worked as a Postdoctoral Fellow with the Chinese University of Hong Kong, a Research Associate with the University of Cambridge, an Assistant Professor and subsequently an Associate Professor with the Nanyang Technological University, Singapore. Currently he is a Visiting Associate Professor with the University of Hong Kong. His research interests include control theory and artificial neural networks, with applications to spacecraft, underwater vehicles, combustion oscillations, microgrids, and smart grids.

M. Z. Q. Chen (M'08) received the B.Eng. degree in electrical and electronic engineering from Nanyang Technological University, Singapore, in 2003, and the Ph.D. degree in control engineering from Cambridge University, Cambridge, U.K., in 2007.

He is currently an Assistant Professor in the Department of Mechanical Engineering at the University of Hong Kong.

Dr. Chen is a Fellow of the Cambridge Philosophical Society and a Life Fellow of the Cambridge Overseas Trust. Since 2008 he has been a reviewer of the IEEE TRANSACTIONS ON AUTOMATIC CONTROL, *Automatica*, *International Journal of Robust and Nonlinear Control*, *International Journal of Adaptive Control and Signal Processing*, *International Journal of Systems Science*, and *Journal of Sound and Vibration*, amongst others. He is now a Guest Associate Editor for the *International Journal of Bifurcation and Chaos*.